

## Dynamical states of underdamped Josephson arrays in a magnetic field

M. Octavio

*Centro de Fisica, Instituto Venezolano de Investigaciones Cientificas, Apartado 21827, Caracas 1020A, Venezuela  
and Center for Superconductivity Research and Department of Physics,  
University of Maryland, College Park, Maryland 20742*

C. B. Whan, U. Geigenmüller, and C. J. Lobb

*Center for Superconductivity Research and Department of Physics,  
University of Maryland, College Park, Maryland 20742*

(Received 30 September 1992)

We present simulations of underdamped classical Josephson arrays in the presence of a magnetic field corresponding to  $f = \frac{1}{2}$  flux quanta per unit cell. We show that the current-voltage characteristics exhibit two distinct regimes. At low voltages, the dynamics are dominated by the motion of the vortex superlattice. At high voltages the dynamics are determined by the breakdown of the individual junctions in the direction of current flow. A rich dynamics is found in the low-voltage region, exhibiting periodic, bifurcating, and complex chaotic solutions. We also present a mechanical analog of the system which helps one to understand the essential features of the simulated dynamics.

The dynamics of completely overdamped Josephson junction arrays, for which the Stewart McCumber parameter  $\beta_c = 2ei_cR^2C/\hbar$  vanishes ( $i_c$ ,  $R$ , and  $C$  are the critical current, shunt resistance, and capacitance of each junction), have been intensively studied in the last two years.<sup>1,2</sup> This interest arises because of the discovery that in the presence of a magnetic field and an rf bias, these arrays exhibit a dynamical state that leads to fractional giant Shapiro steps.<sup>1</sup> Completely overdamped arrays have been preferred experimentally because of the simpler fabrication techniques available for making highly uniform superconducting-normal-superconducting junctions. In simulations,<sup>2</sup> completely overdamped junctions have also been favored because they are described by a first-order differential equation allowing for a faster exploration of parameter space. Experimentally, Van der Zant *et al.*<sup>3</sup> have studied underdamped Josephson arrays in the presence of a magnetic field, but this work concentrated on the study of the properties of the arrays for low numbers of flux quanta per unit cell. The dynamics of a single vortex in an underdamped array has also been investigated theoretically in Refs. 4 and 5.

In this paper we present numerical simulations of the dynamics of underdamped arrays for the fully frustrated case, i.e., for a field such that the number of flux quanta per unit cell  $f = \frac{1}{2}$ . We extend to underdamped arrays the reduced description introduced by Rzchowski, Sohn, and Tinkham<sup>6</sup> which, while approximate, allows for extremely fast exploration of parameter space compared to simulating the full array. We find that the dynamics of underdamped arrays show interesting structure even in the absence of an rf field. As  $\beta_c$  is increased there is significant change in the dc  $I$ - $V$  characteristics, which develop two distinct regimes at low and high voltages. We show that the low-voltage regime arises from the mo-

tion of the vortex superlattice and is thus a flux-flow-like regime. The characteristics switch discontinuously to a high-voltage state in which the junctions in the direction of current flow are in a single-junction-like dc voltage state. We show that the various dynamical regimes in the system can be qualitatively understood in terms of a mechanical analog of a damped particle moving in a two-dimensional potential.

In our simulations, we assume the ground-state symmetry of the system<sup>6,7</sup> for  $f = \frac{1}{2}$  as shown in the inset of Fig. 1(a). The gauge-invariant phase differences  $\alpha$ ,  $\beta$ ,  $\beta'$ , and  $\gamma$  across each of the junctions are each equal to  $\varphi_i - \varphi_j - \psi_{ij}$ , where the  $\varphi_i$  are the phases at the islands connected by a junction,  $\psi_{ij} = (2\pi/\Phi_0) \int_i^j \mathbf{A} \cdot d\mathbf{l}$  is proportional to the line integral of the vector potential  $\mathbf{A}$ , and  $\Phi_0$  is the flux quantum. Since one does not expect a net flow of current, or differences in the phases, in the direction perpendicular to the current flow, the condition  $\beta = \beta'$  is imposed. Each junction is assumed to obey the normalized resistively-capacitively-shunted junction (RCSJ) equation; for example, the junction with phase difference  $\gamma$  in the inset of Fig. 1(a) obeys

$$\beta_c \frac{d^2\gamma}{d\tau^2} + \frac{d\gamma}{d\tau} + \sin \gamma = \frac{i_\gamma}{i_c}, \quad (1)$$

where  $i_\gamma$  is the total current flowing through that junction and  $\tau \equiv (2ei_cR/\hbar)t$  is the dimensionless time. One can then write down three equations for the gauge-invariant phases  $\alpha$ ,  $\beta$ , and  $\gamma$ .

The fluxoid quantization requires for  $f = \frac{1}{2}$

$$\alpha + \gamma + 2\beta = \pi. \quad (2)$$

At the central node, charge conservation gives

$$\begin{aligned}
 -2\beta_c \frac{d^2\beta}{d\tau^2} - 2\frac{d\beta}{d\tau} - 2\sin\beta + \beta_c \frac{d^2\gamma}{d\tau^2} + \frac{d\gamma}{d\tau} + \sin\gamma \\
 + \beta_c \frac{d^2\alpha}{d\tau^2} + \frac{d\alpha}{d\tau} + \sin\alpha = 0. \quad (3)
 \end{aligned}$$

Finally, the total current entering the cell at the left-hand boundary is  $I$ ,

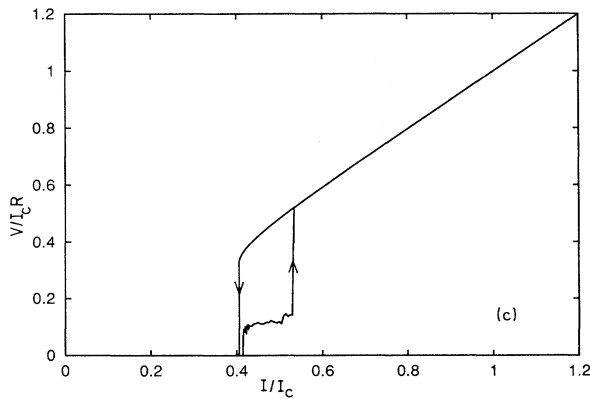
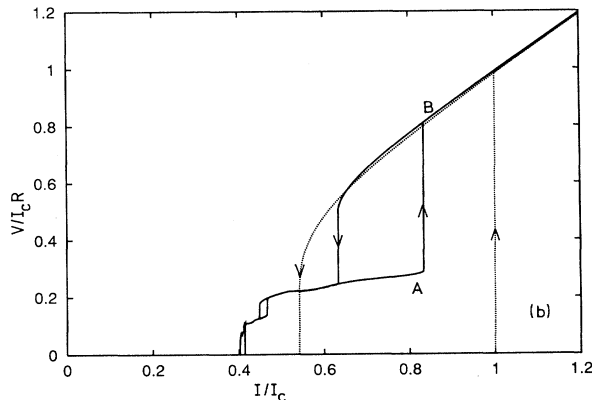
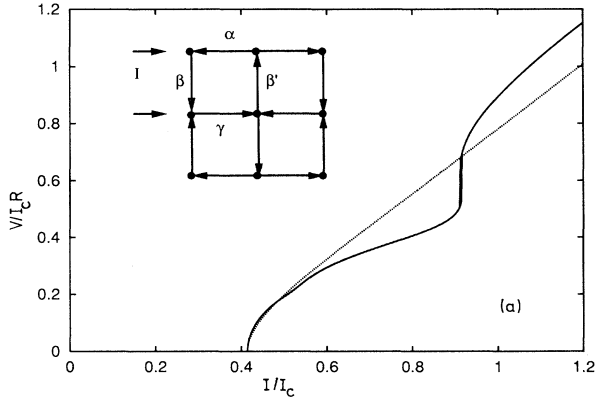


FIG. 1. Normalized dc voltage  $V/I_c R$  as a function of the normalized bias current  $I/I_c$  for four values of  $\beta_c$ . (a)  $\beta_c = 0$  (dotted line) and  $\beta_c = 2$  (full line), (b)  $\beta_c = 5$  (full line), (c)  $\beta_c = 13$ . The inset in (a) shows the definitions of the phase variables for  $f = \frac{1}{2}$  in our reduced-variable description of the infinite lattice, Eqs. (2)–(7). The dotted line in (b) corresponds to a single current biased junction at  $\beta_c = 5$ .

$$\beta_c \frac{d^2\gamma}{d\tau^2} + \frac{d\gamma}{d\tau} + \sin\gamma - \beta_c \frac{d^2\alpha}{d\tau^2} - \frac{d\alpha}{d\tau} - \sin\alpha = \frac{I}{I_c}, \quad (4)$$

where  $I_c = 2i_c$ . It is convenient to use the scaled sum and difference variables  $\xi \equiv (\alpha + \gamma)/\sqrt{2}$  and  $\eta \equiv (\alpha - \gamma)/2$ , for whose motion one finds from Eqs. (2)–(4)

$$\beta_c \frac{d^2\xi}{d\tau^2} = -\frac{\partial U(\xi, \eta)}{\partial \xi} - \frac{d\xi}{d\tau}, \quad (5)$$

$$\beta_c \frac{d^2\eta}{d\tau^2} = -\frac{\partial U(\xi, \eta)}{\partial \eta} - \frac{d\eta}{d\tau}. \quad (6)$$

The potential  $U(\xi, \eta)$  is given by

$$U(\xi, \eta) = -\cos\frac{\xi}{\sqrt{2}} \cos\eta - \sin\frac{\xi}{\sqrt{2}} + \frac{I}{2I_c}\eta. \quad (7)$$

These are also the equations of motion describing a particle of mass  $\beta_c$  sliding down the gradient of the potential  $U$ , its speed being limited by a velocity-proportional frictional force. The different scaling by  $\sqrt{2}$  and 2 in the definitions of  $\xi$  and  $\eta$  is necessary to obtain a diagonal and isotropic “mass” tensor in Eqs. (5) through (6).

Solving Eqs. (5) and (6) is, of course, enormously more efficient than solving the full set of equations for a reasonably sized array.<sup>2,8</sup> We have compared solutions obtained from Eqs. (5) and (6) to those obtained using the full set of equations for  $4 \times 4$  and  $8 \times 8$  arrays. Both the small arrays with the full description and the infinite arrays in the reduced description show similar hysteretic features in the  $I$ - $V$  curves (see below), although there are of course quantitative differences due to finite-size effects.

Figure 1 shows the  $I$ - $V$  characteristics calculated with Eqs. (5) and (6) for four values of  $\beta_c$ : (a)  $\beta_c = 0$  and  $\beta_c = 2$ , (b)  $\beta_c = 5$ , and (c)  $\beta_c = 13$ . In the  $\beta_c = 0$  case the voltage vanishes below the depinning current  $I/I_c = \sqrt{2} - 1 \approx 0.414$ , and then slowly approaches the Ohmic asymptote. For  $\beta_c = 2$  there is already a dramatic change. The  $I$ - $V$  characteristic is now divided into two distinct regions, separated by a discontinuous and hysteretic jump at  $I/I_c \approx 0.915$ . In the low-voltage region the differential resistance depends on the current and on the McCumber parameter, and can be quite complex. Above the jump, the  $I$ - $V$  curve approaches the Ohmic asymptote much faster than for  $\beta_c = 0$ ; the differential resistance is essentially constant.

As  $\beta_c$  is increased to 5 [Fig. 1(b)], the characteristics become even more complex. The differential resistance in the low-voltage region now contains additional structure; in particular, there is a hysteretic jump at  $I/I_c \approx 0.466$ . At the same time, the hysteresis between the low- and high-voltage regions, which was barely discernible for  $\beta_c = 2$ , has become large. For comparison we also show in this figure the  $I$ - $V$  curve of a single junction with the same  $\beta_c = 5$ . In the high-voltage regime, the array response is clearly very close to that of a single junction.

Finally, for  $\beta_c = 13$  [Fig. 1(c)], the lower-voltage region has become rather noisy and quite small in its current range. In fact, we have found an extremely rich and complex chaotic behavior in this lower region<sup>9</sup> for large  $\beta_c$ . It is important to note that in contrast with behavior

ior seen in most Josephson-junction systems, here chaos occurs *without a time-dependent force*.

To understand the difference between the behavior in the two regions, in Fig. 2 we show the normalized *instantaneous* voltages  $-d\alpha/d\tau$  and  $d\gamma/d\tau$  in the direction of the external current [for the two horizontal junctions labeled  $\alpha$  and  $\gamma$  in the inset of Fig. 1(a)] as a function of the dimensionless time. Also plotted is the difference  $-d\eta/d\tau = (d\gamma/d\tau - d\alpha/d\tau)/2$  that is proportional to the voltage across the array. We show two sets of curves, corresponding to currents just below and just above the transition from the low-voltage regime to the high-voltage regime [points A and B in Fig. 1(b)]. Note first that the voltages of the junctions are not in phase. In the low-voltage regime each phase derivative has a large pulse (even more pronounced for lower bias currents) corresponding to the vortex moving across that junction. This region of the  $I$ - $V$  curve is thus dominated by the motion of the vortex superlattice in the direction perpendicular to the applied current, and may be called a flux-flow-like regime. The voltage wave forms for the same junctions just above the jump, in the upper region, are still out of phase, but otherwise look like single-junction characteristics, in accordance with the resulting dc voltage closely resembling that found for a single junction [compare Fig. 1(b)]. Note that most of the voltage across each junction is dc, and the oscillation is only a small fraction of the total voltage.

Further physical insight can be obtained from the equivalence of Eqs. (5) and (6) to the equation of motion of a particle. In Figs. 3(a) and 3(b) we plot the potential given by Eq. (7) together with two trajectories. The tilt of the potential in the  $-\eta$  direction is proportional to the applied current, while the velocity of the particle in the  $-\eta$  direction is proportional to the voltage across the array. For low  $\beta_c$  the frictional force dominates, and the particle follows the gradient of the potential. For  $I/I_c < \sqrt{2} - 1$  the potential has local minima, in which the particle can be trapped (vortex pinning).

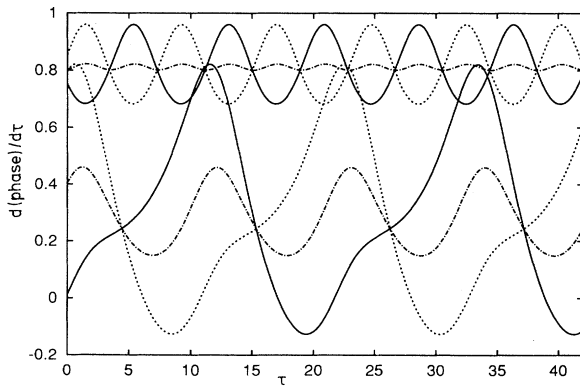


FIG. 2. Normalized instantaneous voltages  $d\gamma/d\tau$  (full lines) and  $-d\alpha/d\tau$  (dotted lines) as functions of the dimensionless time  $\tau$ . The lower one of each type of curve corresponds to  $I/I_c = 0.832$ , the upper one to  $I/I_c = 0.835$  [points A and B in Fig. 1(b)]. Also shown is  $-d\eta/d\tau = (d\gamma/d\tau - d\alpha/d\tau)/2$  (dashed-dotted lines), which is proportional to the voltage across the array.

With increasing  $\beta_c$  the influence of inertia grows, and the path of the particle now also contains parts moving uphill. The trajectories exhibit a surprising complexity; they become unstable at certain current values, where they change qualitatively and a jump in the  $I$ - $V$  curve occurs (e.g., at  $I/I_c \approx 0.466$  for  $\beta_c = 5$ ). Trajectories in the noisy regime of Fig. 1(c) look erratic. These chaotic solutions are quite interesting: rather than being oscillations of random amplitude occurring every period, they are random amplitude fluctuations at random time intervals. A detailed study of this behavior will be described elsewhere.<sup>9</sup>

The large hysteretic jump between the low-voltage regime and the high-voltage regime is the analog of the so-called “row-switching” phenomenon observed in systems with sparse vortices.<sup>3,4</sup> This jump can be quite easily understood in the mechanical visualization of the system. In the low-voltage region, the particle more or less follows the “side valleys” of the potential. With increasing current and the McCumber parameter, however, the trajectory moves closer and closer to the crest of the “hill” separating two side valleys in the  $\eta$  direction [see Fig. 3(a)]. At the jump, the particle is fast enough to overcome the hill. It no longer has to follow the side valleys, allowing its speed in the  $-\eta$  direction, the voltage, to increase and to become nearly uniform [cf. Figs. 3(b) and 2].

When an ac component is added to the applied cur-

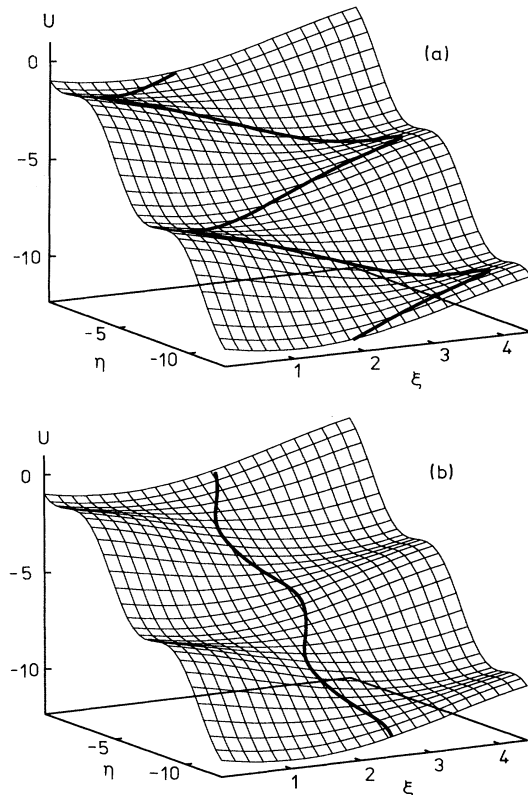


FIG. 3. Trajectories and the potential  $U(\xi, \eta)$  of Eq. (7) for  $\beta_c = 5$ . (a)  $I/I_c = 0.832$  and (b)  $I/I_c = 0.835$  [corresponding to the points A, B in Fig. 1(b)].

rent, Shapiro steps show up in the  $I$ - $V$  characteristic. The mechanical analog can also help to understand their properties. That is already true for the overdamped case, where half-integer Shapiro steps were observed in fully frustrated arrays both in experiment<sup>1</sup> and in subsequent numerical studies.<sup>2,6,8</sup> This observation first came as a surprise, since half-integer steps, where their phases move by  $2\pi$  in two periods of the ac drive, are absent in a single overdamped junction.<sup>10</sup> But in the fully frustrated array, along trajectories of the type shown in Fig. 3(a), the period of  $\dot{\eta}$  (to the integral of which the applied current couples) is half that of the individual phases. In this sense a half-integer step of the  $f = \frac{1}{2}$  array corresponds to an integer step of a single junction, making the occurrence of the half-integer steps plausible. However, the additional  $\xi$  degree of freedom present in the array allows for a deformation of the trajectories under influence of the ac bias that has no counterpart in a single junction. On half-integer steps, the trajectories must stay symmetric with respect to the line  $\xi = \pi/\sqrt{2} \approx 2.22$ , where the potential modulation in the  $\eta$  direction vanishes, in order to keep the  $\dot{\eta}$  period along the trajectory equal to half the period of the individual phases. This is not required for integer steps, on which indeed the trajectories become asymmetric with respect to  $\xi = \pi/\sqrt{2}$  and move into a region to the right or to the left of this line, where the potential modulation in the  $\eta$  direction is larger. With increasing applied frequency the dc current on the Shapiro step grows, and the potential gradient points mainly in the  $-\eta$  direction, so that the  $\xi$  oscillations of the trajec-

tories become small. On half-integer steps the potential modulation in the  $\eta$  direction therefore rapidly becomes small with increasing frequency. This explains why the size of the half-integer steps decreases faster with increasing frequency than that of the integer steps, as observed in Refs. 6 and 8.

In the underdamped case the depression of the half-integer steps becomes even more pronounced,<sup>9</sup> as the voltage corresponding to the  $\frac{1}{2}$  step moves across the jump from the low- to the high-voltage regime [from point A to point B in Fig. 1(b)]. This can again be understood as a consequence of the reduced potential modulation in the  $\eta$  direction along the trajectories, which is obvious from Figs. 2 and 3.

In conclusion, we have presented simulations of the dynamics of underdamped Josephson-junction arrays for half a flux quantum per plaquette. We show that the system may exhibit complex dynamical states, which are directly reflected in the  $I$ - $V$  characteristics. Many features may be understood qualitatively in a mechanical analog. They have yet to be observed in experiments.

We are grateful to F. Wellstood for useful comments. This work was supported in part by the AFOSR through Grant No. F49620-92-J-0041, the NSF through Grant Nos. DMR-8901723 and INT-9202471, and through CONICIT. One of us (M.O.) acknowledges support from the Guggenheim Foundation during the course of this work, and U.G. was supported by NATO.

<sup>1</sup>S.P. Benz, M.S. Rzchowski, M. Tinkham, and C.J. Lobb, Phys. Rev. Lett. **64**, 693 (1990); H.C. Lee, R.S. Newrock, D.B. Mast, S.E. Hebboul, J.C. Garland, and C.J. Lobb, Phys. Rev. B **44**, 921 (1991); L.L. Sohn, M.S. Rzchowski, J.U. Free, S.P. Benz, M. Tinkham, and C.J. Lobb, *ibid.* **44**, 925 (1991).

<sup>2</sup>S. Chung, K.H. Lee, and D. Stroud, Phys. Rev. B **40**, 6570 (1989); K.H. Lee, D. Stroud, and J.S. Chung, Phys. Rev. Lett. **64**, 962 (1990); J.U. Free, S.P. Benz, M.S. Rzchowski, M. Tinkham, C.J. Lobb, and M. Octavio, Phys. Rev. B **41**, 7267 (1990); D. Domínguez, J.V. José, A. Karma, and C. Wiecko, Phys. Rev. Lett. **67**, 2367 (1991).

<sup>3</sup>H.S.J. van der Zant, F.C. Fritschy, T.P. Orlando, and

J.E. Mooij, Phys. Rev. Lett. **66**, 2531 (1991); Europhys. Lett. **18**, 343 (1992).

<sup>4</sup>U. Geigenmüller, C.J. Lobb, and C.B. Whan, Phys. Rev. B **47**, 348 (1993).

<sup>5</sup>U. Eckern and E.B. Sonin, Phys. Rev. B **47**, 505 (1993).

<sup>6</sup>M.S. Rzchowski, L.L. Sohn, and M. Tinkham, Phys. Rev. B **43**, 8682 (1991).

<sup>7</sup>S. Teitel and C. Jayaprakash, Phys. Rev. B **51**, 1999 (1983); T.C. Halsey, *ibid.* **31**, 5728 (1985).

<sup>8</sup>M. Octavio, J.U. Free, S.P. Benz, R.S. Newrock, D.B. Mast, and C.J. Lobb, Phys. Rev. B **44**, 4601 (1991).

<sup>9</sup>M. Octavio, C.B. Whan, and C.J. Lobb (unpublished).

<sup>10</sup>M.J. Renne and D. Polder, Rev. Phys. Appl. **9**, 25 (1974).